ALL-FIBER OPTICAL PARAMETRIC OSCILLATOR FOR COHERENT RAMAN IMAGING

A Thesis

Presented to the Faculty of the Graduate School

of Cornell University

in Partial Fulfillment of the Requirements for the Degree of

Master of Science

by

Hanzhang Pei

May 2015

ABSTRACT

Optical parametric oscillator (OPO) is a kind of light source similar to a laser but based on parametric gain from amplification in a nonlinear medium rather than from stimulated emission. It features wide frequency tunability and high power narrow linewidth output, which enables its application to laser spectroscopy and atom-light interaction. Although OPOs could provide two synchronized pulse trains for coherent anti-Stokes Raman spectroscopy (CARS) imaging, they remain bulky and sensitive tools requiring careful alignment, making these devices unpractical for surgical situations. Thus, all-fiber source for coherent Raman imaging have generated interest among clinical researchers and doctors. Thanks to recent advances in the understanding of nonlinear pulse evolution in optical fibers and engineering of PCF structures, fiber-based OPOs have achieved performance comparable to conventional solid-state devices.

This thesis discussed the previous effort towards an all-fiber source of pulses for use in CARS imaging, as well as principles behind picosecond pulse generation and coherent Raman imaging. An all-fiber OPO pumped by commercial solid state laser and divided pulse amplifier is demonstrated based on frequency conversion of picosecond pulses through four-wave mixing process in customized photonic crystal fiber. This will be another step further towards an all-fiber device for coherent Raman microscopy.

BIOGRAPHICAL SKETCH

Hanzhang Pei was born in Hefei, China in 1992. Before his family moved to urban area, he spent his entire childhood in the countryside where he first appreciated the beauty of nature. At the age of 16, he headed north to the nation's "Ice City" Harbin to join the inaugural Elite Student Program at Harbin Institute of Technology. Apart from his coursework and research on metamaterials and hydrophones, he devoted the majority of his undergraduate life to the institute's Model United Nations association, which shaped his future career goal as an entrepreneur. He received his bachelor's degree in Optics in 2013.

Not content with his knowledge reserve then, he attended the Applied Physics master program of Cornell University, where he rediscovered the joy of science. After exploring 3D printing technologies with Prof. Robert Thorne and instructing multiple optics labs, he joined the Wise Research Group to develop an all-fiber source for coherent Raman imaging.

His journey will continue in Professor Almantas Galvanauskas' group at University of Michigan as a PhD student in Electrical Engineering. (It seems he has a bizarre affection of snow and ice.) There he will be working on high power ultrafast lasers and their application to compact particle accelerators.

To my parents, Tommy and Grace for their support, companionship and love.

ACKNOWLEDGEMENTS

I would first like to thank Prof. Frank W. Wise for his support as my thesis advisor. His tremendous effort on tracking each group member's status and providing suggestions and guidance to the best of his knowledge is very impressive. His advice not only lies on experiment details but more importantly on grasping the big picture tightly, which would certainly affect my thinking pattern in a long run. Also, he is very supportive for my pursuit of doctoral research at other universities after masters study, which I really appreciate. I am very grateful for the scientific and ideological training I have received under his supervision.

Meanwhile I would like to sincerely thank Erin for her guidance throughout my research project. I have learned so much on experiment designs and conduction as well as important concepts from her. She is so resourceful, helpful and responsible, making her a model citizen of the research group. I also thank Yuxing for his technical support on my experiments and Logan for his advice on future career plans. I thank National Science Foundation and National Institutes of Health for funding this research project, and Bath University for providing the customized photonic crystal fiber.

My gratitude also extends to my AEP peers Daiwei, Will, Pengzi, Megnan, Xincheng, Daniyar, Chengyu, Xiaoyue, Yimo and Shuishen, my friends here Chen, Wenjin, Suki and Ying, as well as distant friends including Lecheng, Jiahan and Yao; you have made my days at Cornell colorful and pleasant.

Finally, I specially thank Tommy for his companionship throughout our undergraduate and masters study and Grace for her accompany. I wholeheartedly thank my parents for supporting any of my decisions.

TABLE OF CONTENTS

LIST OF TABLES

LIST OF FIGURES

CHAPTER 1

INTRODUCTION & MOTIVATION

1.1 Introduction & Previous Work

Optical parametric oscillator(OPO) is a kind of harmonic oscillator whose parameters oscillate at optical frequencies. It could function like a light source similar to laser, but its optical amplification is based on optical gain from parametric amplification in nonlinear medium instead of stimulated emission. It is also an ideal source to generate tunable ultrashort pulses.

One of the most valuable features of OPO is that its amplified output frequency is tunable in a broad range, which is desirable for many applications including laser spectroscopy and Raman imaging. To achieve this, we need to change the solution of ω_s for perfect phase matching condition, and angle tuning turns out to be a plausible approach. The effective second second-order nonlinearity is orientation-dependent, e.g. for Potassium titanyl phosphate(KTP) d_{eff} is approximated by

$$TypeI : d_{eff} = \frac{1}{2}(d_{15} - d_{24})sin(2\theta)cos(2\phi), \tag{1.1}$$

$$TypeII : d_{eff} = -(d_{15}sin^2(\phi) + d_{24}cos^2(\phi))sin(\theta), \tag{1.2}$$

hence d_{eff} could be maximized with appropriate spacial angles θ and ϕ[15]. As we adjust the orientation of nonlinear medium, its extraordinary refractive of index changes, leading to a corresponding deviation of phase matching condition solution. Temperature tuning may also work for materials with strongly temperature-dependent birefringence, as shown in Figure 1.1, where the potential applied to the crystal was ramped repetitively at fixed temperature and the

output wavelength measurements were repeated at incrementally changed temperatures. The double resonant OPO(DRO) output directed into the monochromator consists of a series of pulses. The radiation transmitted by the monochromator usually consisted of narrow pulses that are able to be correlated with the electric potential applied to the DRO electrodes[5].

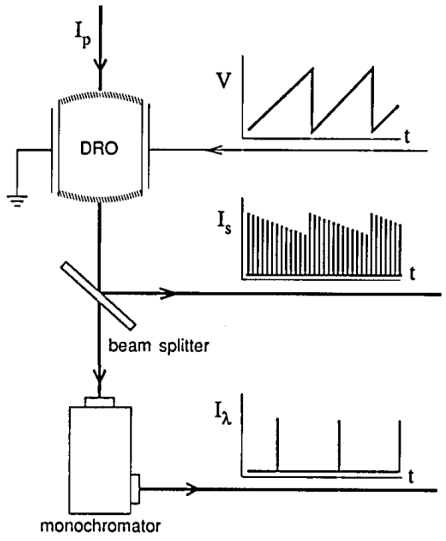

Figure 1.1: Schematic of the DRO tuning measurements [5].

The signal and idler signals from synchronously pumped OPO provide the two colors for coherent anti-Stokes Raman scattering (CARS) microscopy. The OPO is continuously tunable over a broad range of Raman shifts of 100-3700cm^{-1} by varying the temperature of the nonlinear crystal. The near-infrared output at 900 - 1300 nm allows deep penetration into samples and reduced nonlinear photodamage[8]. Feruz Ganikhanov, et.al. demonstrated a simple laser source for CARS microscopy that meets the requirements of being a compact laser system that has broad tunability with optimized spatial resolution, penetration depth, and nonlinear photodamage. The experimental setup is shown in

Figure 1.2:

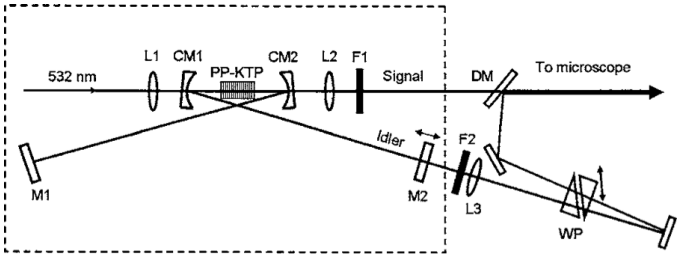

Figure 1.2: OPO resonator and external layout for CARS microscopy [8].

One elegant way to make OPOs more accessible and integrated is to take advantage of the compact and alignment-free nature of fiber. The conventional resonant cavity approach requires a complicated cavity alignment for regenerative oscillation and phase matching, thus fiber optical parametric oscillators (FOPOs) based on four-wave mixing process inside optical fibers have attracted considerable attention.

The first clear demonstration of a broadly tunable short-pulse FOPO in near-infrared regime is by Yujun Deng, et.al. who reported a photonic-crystal-fiber-based parametric oscillator producing pulses as short as 460 fs and a tuning range of 200 nm around 1μm[4]. The ring cavity with 65 cm photonic crystal fiber (PCF) is synchronously pumped by a passively mode-locked Yb-doped fiber laser. Due to high-order dispersion in the photonic crystal fiber, using the modulation instability gain in normal dispersion could convey widely extended tunability. By turning the intracavity grating and rematching the cavity length, the signal wavelength is tunable over 140 nm on the longer wavelength side (1060 - 1200 nm), as shown in Figure 1.3, where the smaller peak at 1090 nm in the first trace is a cascaded FWM component, and the component near 977 nm is the residual diode pump light leaking through the FOPO.

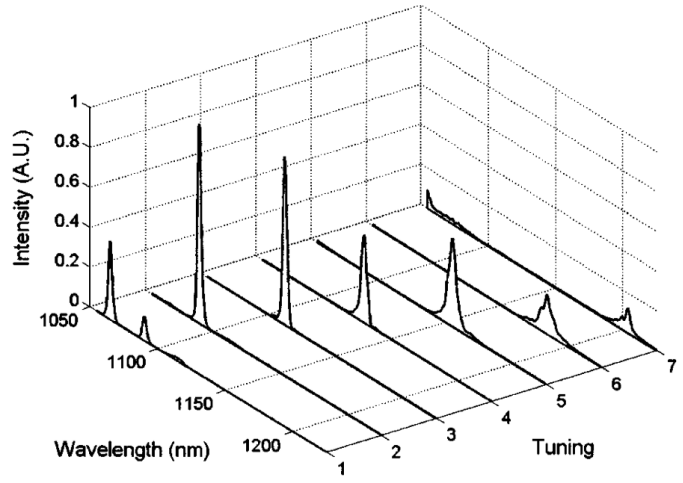

(a)

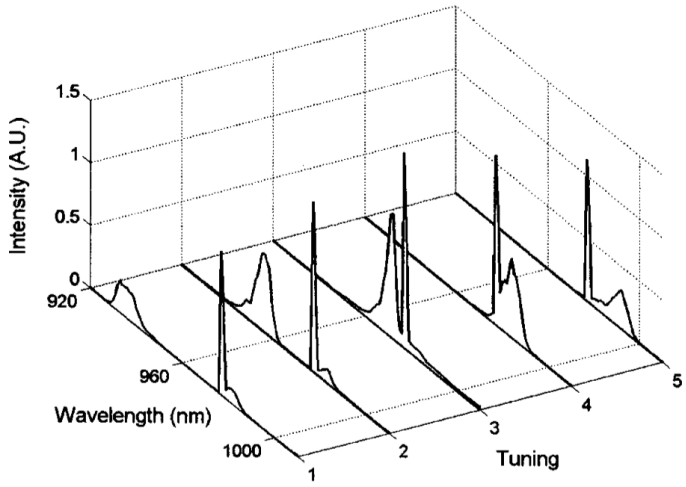

(b)

Figure 1.3: (a) Signal wavelength tuning on the longer wavelength side of the pump. (b) Idler wavelength tuning on the shorter wavelength side of the pump [4].

Khanh Kieu, et.al. built an integrated fiber source of high-energy transform-limited picosecond pulses, as demonstrated in Figure 1.4. The 1030 nm pulses from the fiber source are frequency doubled through sum frequency generation (SFG), and the resulting pulses at 515 nm pump an OPO, which provides two tunable pulse trains for CARS imaging [10]. Compared with picosecond

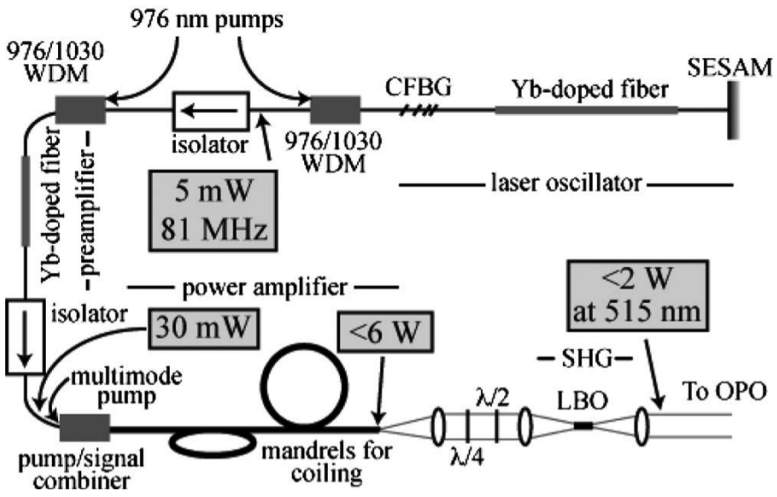

Figure 1.4: Schematic of the picosecond laser system[10].

solid-state lasers for CRM [8], this fiber source offers shorter pulses and special features of being air cooled and compact. This was the first step towards an all-fiber source for CARS imaging.

However, limited pulse energy yields peak powers lower than from that of conventional solid-state systems. Thus a major challenge is finding a fiber-based pulse source scalable to high powers. Four-wave mixing (FWM) in PCF has been used to convert picosecond pulses with duration of 100-200 ps to large frequency shifts. For few-picosecond pulses, interaction length is on the order of tens of centimeters due to group-velocity mismatch (GVM), which limits unseeded FWM conversion. Thus Simon Lefrancois, et.al. presented a fiber-based picosecond source for CARS microscopy, as shown in Figure 1.5.

Here, frequency conversion is completed through FWM in normal-dispersion photonic crystal fibers. Seeding the process largely reduces GVM and suppresses noise. Pulses from a 1μm fiber amplifier are converted to around 800 nm with average power up to 160 mW and durations around 2 ps. Frequency shifts in the range of 2650 to 3200cm^{-1} have been achieved [14]. The

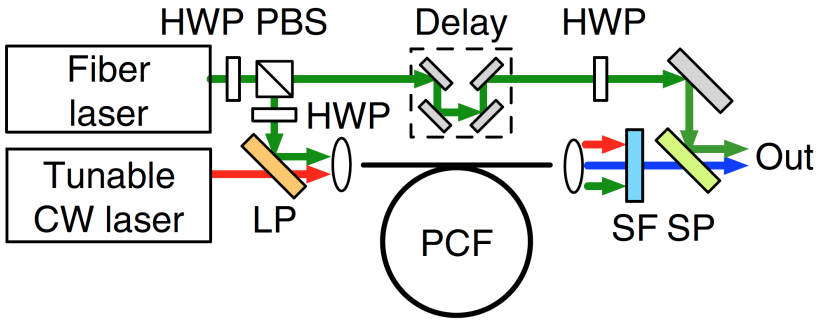

Figure 1.5: Experimental setup of the fiber FWM source[14].

OPA structure generated signal pulses with 166 mW average power and 1.8ps duration, while 308 mW pump pulses are picked off. This system successfully demonstrated its application to imaging mouse brain and skin tissues, as well as single cells. This was the first fiber instrument offering performance comparable to solid state systems.

To solve the problem that output optical parametric amplification has a relatively low conversion efficiency and FWM tends to create noisy signal pulses, a synchronously pumped fiber optical parametric oscillator based on the normal dispersion of FWM process is proposed [11]. Erin S. Lamb, et.al. claimed that filtering the field fed back into the photonic crystal fiber(PCF) results in stable, narrow-band operation, which in turn stabilizes both signal field and idler field in the oscillator. Relative intensity noise(RIN) could also be reduced significantly due to self-consistent nature of OPO. The OPO achieves similar pulse parameters of 2 - 4 ps duration and 3 - 4 nJ pulse energy to the OPA of [14], but with significant performance and practical advantages over the previous OPA design. One the one hand, the self-consistent nature of the OPO results in substantial reduction of the relative intensity noise (RIN) on the output signal. One the other hand, the OPO reaches 13%-20% conversion efficiency to the sig-

nal wavelength, as compared to only 10% in the OPA. As a practical advantage, this OPO design eliminates the external CW seed laser used in [14].

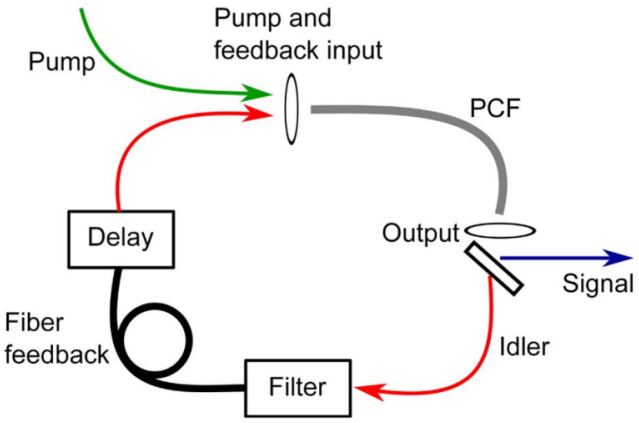

Figure 1.6: Schematic of PCF-based OPO[11].

The experimental setup is depicted in Figure 1.6. A Yb-doped fiber laser supported divided-pulse amplifier generates pulses that are coupled into the PCF and converted into signal and idler pulses. The signal pulses are coupled out with a dichroic mirror, and idler pulses pass through a Gaussian filter and are delayed to synchronize with pump pulses, yielding stable operation of the OPO. The frequency shift between the pump and signal can be tuned by adjusting the center of the filter which consists of a diffraction grating and a fiber collimator. Tuning the seed oscillator enables a broader frequency tuning range.

Recently, Thomas Gottschall, et.al. has developed a fiber-based CARS laser source based on four-wave-mixing (FWM). In order to enhance its spectral resolution and efficiency, a FWM based FOPO is presented. This source provides 180 mW average power with 5.6 kW peak power of the CARS pump and 130 mW average power with 2.9 kW peak power for the Stokes signal. CARS resonances around $2850cm^{-1}$ and $2930cm^{-1}$ can be resolved with a spectral resolution

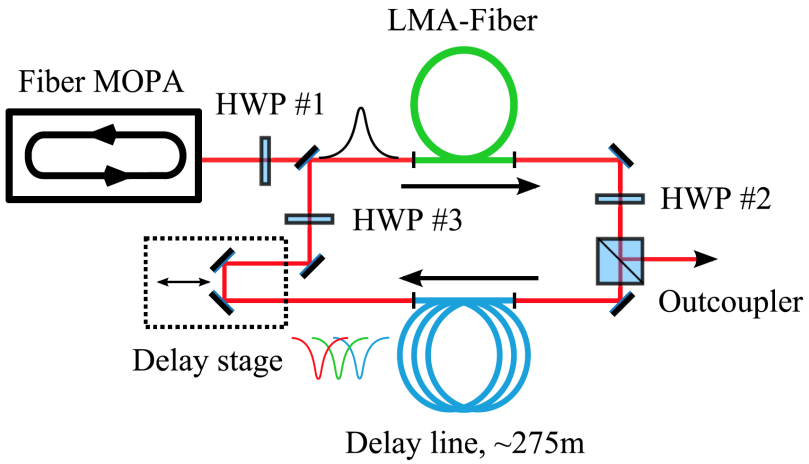

Figure 1.7: Schematic setup of the FWM-based CARS Source[9].

of $1cm^{-1}$, which enables high-contrast, spectrally resolved CARS microscopy of biological tissues [9].

Christian W. Freudiger, et.al. developed a robust fiber laser source for SRS microscopy. Starting with an Er-doped fiber oscillator mode-locked with a carbon nanutube (CNT) saturable absorber, two synchronized beams are split and sent into two arms to generate pump and Stokes beams. In one arm, the beam is amplified to 80mW and spectrally filtered to reduce broadened bandwidth due to self-phase modulation (SPM), and then it is frequency doubled to serve as the near-infrared pump beam at 790nm. In the other arm, super-continuum is generated then filtered to the 1015 nm to 1045 nm tunable range with less than 0.1nm tuning accuracy. Together with balanced detection scheme, intensity noise from fiber source is mostly eliminated, providing a quiet enough synchronized pulse source for SRS microscopy [7].

1.2 Motivation

Coherent anti-Stokes Raman scattering (CARS) microscopy is a kind of label-free biological imaging by exciting molecular vibrations [6]. However, it requires two synchronized pulse trains with picosecond durations and bandwidths smaller than the Raman linewidth and a frequency difference tunable to the desired Raman shift. The FWM signal pulses generated by OPO's, together with pump residual signals, could be applied on coherent Raman imaging, including coherent anti-Stokes Raman scattering(CARS) and also stimulated Raman scattering(SRS). An example SRS microscopy setup is shown in Figure 1.8:

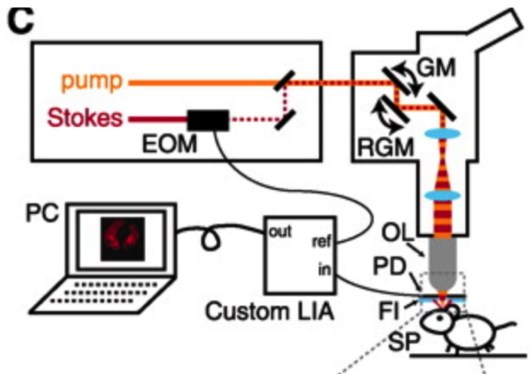

Figure 1.8: Experimental setup for in vivo SRS microscopy detected the intensity transfer from the Stokes beam to the backscattered pump beam[17].

where the specimen is excited by focusing light with an objective lens through a small pinhole in the center of the large-area epi-detector (PD). Scattering effect within the tissue sample redirects a large portion of the forward-traveling light which is detected by PD. The 10MHz modulated Stokes beam is blocked by a filter, whereas the transmitted pump beam is detected and demodulated by the Locked-in Amplifier (LIA). Images are constructed by 2D scanning the focal

spot with the laser-scanning system consisting of a galvanometer mirror (GM) and a resonant galvanometer mirror (RGM) [17].

The main motivation we have is a strong need for an all-fiber light source for coherent Raman imaging from Houston Methodist™. A list of desired parameters for such fiber source is shown in Table 1.1:

Table 1.1: Fiber source requirements from Houston Methodist™

Laser Pulse Duration	1ps - 10ps
Pump Pulse	817nm, 1.0nm
Stokes Pulse	1064nm, 1.4nm
Repetition Frequency	Tens of MHz
Laser Power	200mW
Synchronization	Yes
Size	$10'' \times 18''$

Such light source should fit in a typical surgical cart, as shown in Figure 1.9, which also demonstrates a CARS endoscope system. Optical resources with Solid state components, typically including mirrors and lenses, are unpractical for brain surgeries where a real-time in-vivo imaging device is needed, and thus we are motivated to bring the previous developed PCF-based OPO [11] to an all-fiber OPO, which will potentially serve as a compact and alignment-free light source for CARS imaging in clinical uses. This will be one more step towards all-fiber coherent Raman microscopy source goal.

Figure 1.9: Illustration of CARS endoscope system. 1: display; 2: optical source; 3: optical detector; 4: control & acquisition system; 5: fiber optic probe.

CHAPTER 2

THEORETICAL BACKGROUND

2.1 Optical Parametric Oscillator

2.1.1 Difference Frequency Generation

To better understand what happens during this process, we may first take a step away from the subject and get through a few concepts. Media including crystals, water, air and even vacuum are essentially nonlinear, and their nonlinear properties can be characterized as higher order susceptibilities. Because of such nonlinearity, the responding polarization is a power series in the field strength $\tilde{E}(t)$

$$\tilde{P}(t) = \epsilon_0[\chi^{(1)}\tilde{E}(t) + \chi^{(2)}\tilde{E}^2(t) + \chi^{(3)}\tilde{E}^3(t) + ...]. \tag{2.1}$$

Consider an optical field incident on the nonlinear medium consisting of two frequency components ω_1 and ω_2, the higher-order terms in Equation 1 will generate new frequencies including $(\omega_1 - \omega_2)$ component

$$P(\omega_1 - \omega_2) = 2\epsilon_0\chi^{(2)}E_1E_2^*. \tag{2.2}$$

This nonlinear physical process is called *Difference Frequency Generation(DFG)*, and it is the main principle behind $\chi^{(2)}$ OPO. A schematic of difference frequency generation is shown in Figure 2.1.1 [2].

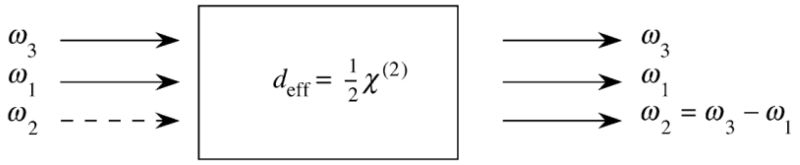

Figure 2.1: Difference frequency generation

2.1.2 Optical Parametric Amplification

Through the wave equation derived from Maxwell's Equations, we may solve for the amplitude of output signal field

$$A_1(z) = [A_1(0)(cosh(gz) - \frac{i\Delta k}{2g}sinh(gz)) + \frac{\kappa_1}{g}A_2^*(0)sinh(gz)]^{e^{i\Delta kz/2}}, \tag{2.3}$$

where we introduces quantities

$$g = [\kappa_1\kappa_2^* - (\frac{\Delta k}{2})^2]^{\frac{1}{2}}, \quad \kappa_1 = \frac{2i\omega_i^2 d_{eff}A_3}{k_1c^2}. \tag{2.4}$$

The term $\Delta k = k_3 - k_1 - k_2$ is called the *wavevector mismatch*. For the special case $\Delta k = 0$, also known as *perfect phase matching condition*, the field amplification is maximized as g is a sinc function with respect to Δk, and light experiences monotonic growth as it propagates through the material.

A schematic of optical parametric amplification is shown in Figure 2.2(a) [5]. It converts an input pump wave ω_p into two output waves of lower frequencies whose frequency sum equals to the input wave frequency. The two output frequencies ω_s and ω_i are called "signal" and "idler" respectively, depending on which is the desired component to be amplified.

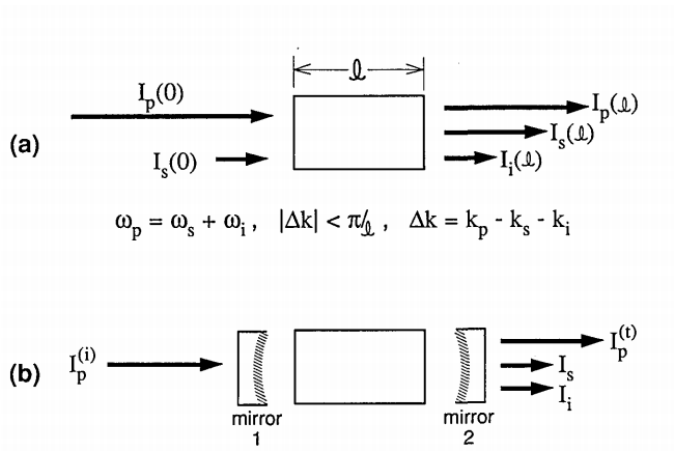

Figure 2.2: (a). Optical parametric amplification (b). Optical parametric oscillator

2.1.3 Optical Parametric Oscillator

Figure 2.2(b) shows a typical setup of OPO, where the two mirrors are highly reflective at a certain frequency range. If the device is resonant at both frequencies ω_s and ω_i, then it's called a doubly resonant oscillator; if the device is highly resonant at either ω_s or ω_i but not both, then it's known as a singly resonant oscillator.

To generate ultrashort pulses using OPO, synchronous pumping is the only approach since parametric processes cannot store pump energy for later use. The pump light is delivered in the form of ultrashort pulses that are synchronized with the pulses circulating in the device instead of in the form of continuous pumping waves like mode-lock laser [16]. Such synchronization requires a precise match of the repetition rate of pump pulse and the round-trip frequency of the resonator. Synchronously pumped optical parametric oscillator is widely used to produce ultrashort pulses with tunable wavelength [18].

2.2 Four Wave Mixing

Four wave mixing is a nonlinear process which results from frequency mixing by third-order nonlinear response $\chi^{(3)}$, where three waves mix to generate a fourth wave at a new frequency. Conservation of energy and conservation of momentum are the two major factors that determines the outcome o this parametric mixing process, as described in Eqs. . The photon energy is $\hbar\omega$ and the photon momentum is $\hbar k$, where the wavevector $k = 2\pi n(\omega)/\lambda$, with $n(\omega)$ is the effective refractive index.

$$\hbar\omega_1 + \hbar\omega_2 = \hbar\omega_3 + \hbar\omega_4 \tag{2.5}$$

$$\Delta k = k_1 + k_2 - k_3 - k_4 = 0 \tag{2.6}$$

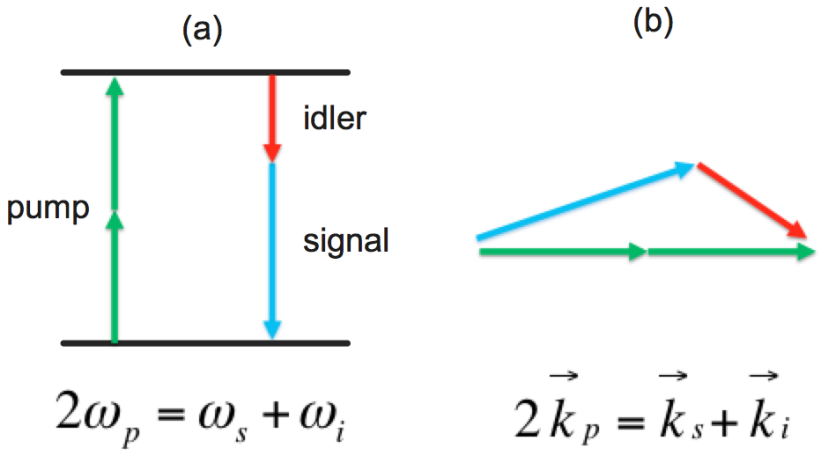

Figure 2.3: Degenerate Four Wave Mixing. (a). Conservation of energy (b). Conservation of momentum

Here we are interested in degenerate FWM process where $\omega_1 = \omega_2$. In other words, two pump photons mix to generate a signal photon and an idler photon pair, as shown in Figure 2.3.

The phase-matched gain spectrum depends on the non-linear phase shift γP_0 and the net phase-mismatch κ:

$$g = \sqrt{(\gamma P_0)^2 - (\kappa/2)^2}, \tag{2.7}$$

$$\kappa = 2\gamma P_0 + 2\sum_{i=1}^{\infty} \frac{\beta_{2n}}{(2n)!}(\omega - \omega_0)^{2n}. \tag{2.8}$$

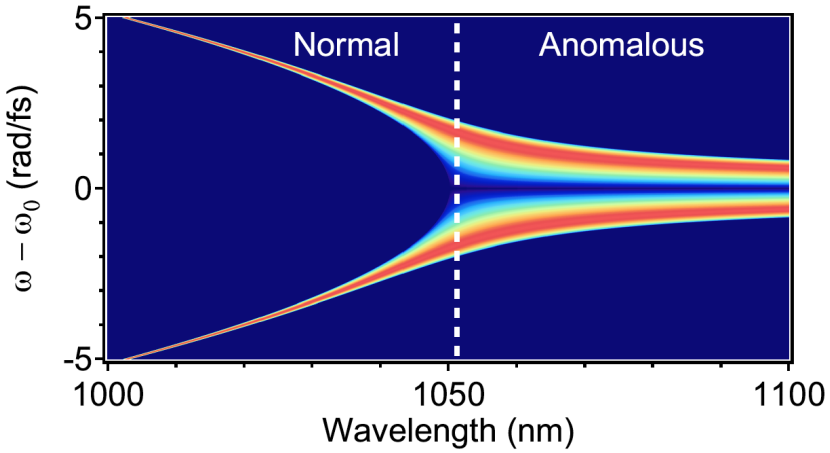

Figure 2.4: Typical gain spectrum of degenerate Four Wave Mixing[13].

Figure 2.4 shows a typical example of the FWM gain spectrum. At anomalous dispersion regime, g is maximized when the GVD β_2 and the SPM γP_0 cancel. The FWM sidebands are broad and close to the pump, which enables modulation instability at anomalous dispersion. At normal dispersion, the GVD and SPM add up. Higher order dispersion terms are thus necessary to obtain phase matching, causing narrow bands aside the pump frequency.

Phase-matching condition in optical fibers can be satisfied by self-phase modulation, the index difference in birefringent optical fibers and intermodal dispersion in multimode fibers [1]. Photonic crystal fibers have specially engineered waveguide dispersion so that FWM phase-matching tunability is achieved.

Since the FWM phase-matched gain in optical fibers is dependent on the dispersion properties of the fiber, phase matching yields widely-spaced and narrow sidebands at normal dispersion, as required for CARS. Position of signal-idler pair can be controlled by engineering the dispersion of a PCF, especially at its zero dispersion wavelength. For our experiment, a custom PCF was provided by our collaborators at Bath University (Fiber 050803B). The fiber is endlessly single-mode with a one missing hole design, so the spontaneous FWM sidebands obtained around 1030 nm were observed at wavelengths suitable for CARS microscopy [13]. Figure 2.5 shows a cross-section of the fiber as well as a modeled dispersion curve to match the observed FWM wavelengths.

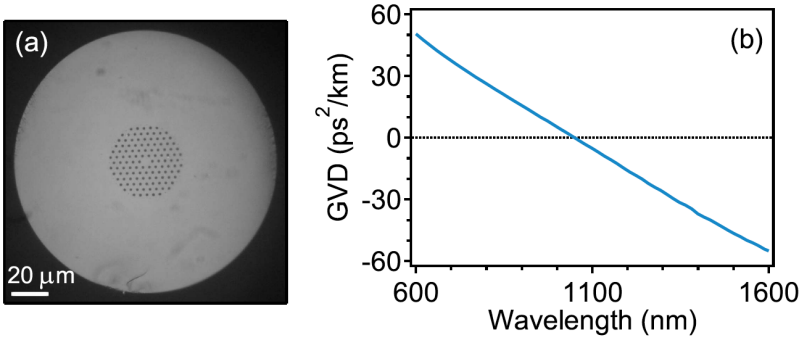

Figure 2.5: Fiber 050803B cross section and modeled dispersion curve[13].

The phase matching diagram of this PCF can be calculated by Eqs.2.7 - 2.8, where the dispersion coefficients β_n come from the dispersion curve of fiber 050803B, as shown in Figure 2.6. This diagram indicates that a pump pulse laser at 1030nm to 1040 nm can be shifted to 770nm to 820nm wavelength range with narrow bandwidths through FWM process in the customized PCF.

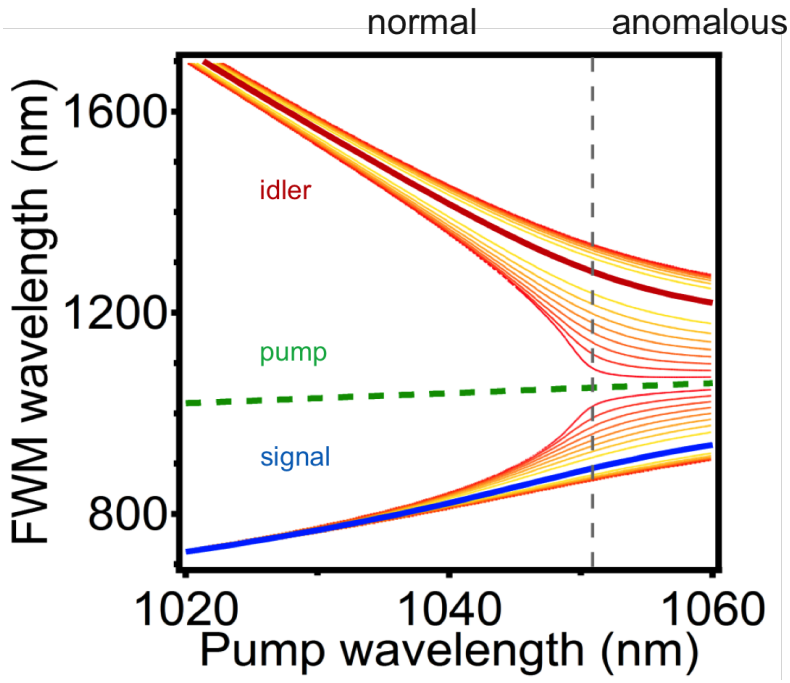

Figure 2.6: Fiber 050803B phase matching diagram.

2.3 Coherent Raman Imaging

2.3.1 Coherent Anti-Stokes Raman Scattering Microscopy

The signal pulses could be applied on coherent Raman imaging, including coherent anti-Stokes Raman scattering(CARS) and stimulated Raman scattering(SRS). CARS is a four-wave mixing process where a pump field $E_p(\omega_p)$, a Stokes field $E_s(\omega_s)$ and a probe field $E_p^{'}(\omega_p^{'})$ interact with the detected sample and generate an anti-Stokes field $E_{as}(\omega_{as})$ at the frequency $\omega_{as} = \omega_p - \omega_s + \omega_p^{'}$ [3]. The energy diagram of CARS is depicted in Figure 2.7.

In CARS microscopy, the temporally and spatially overlapped pump and Stokes beams are tightly focused into a sample to generate anti-Stokes signal in

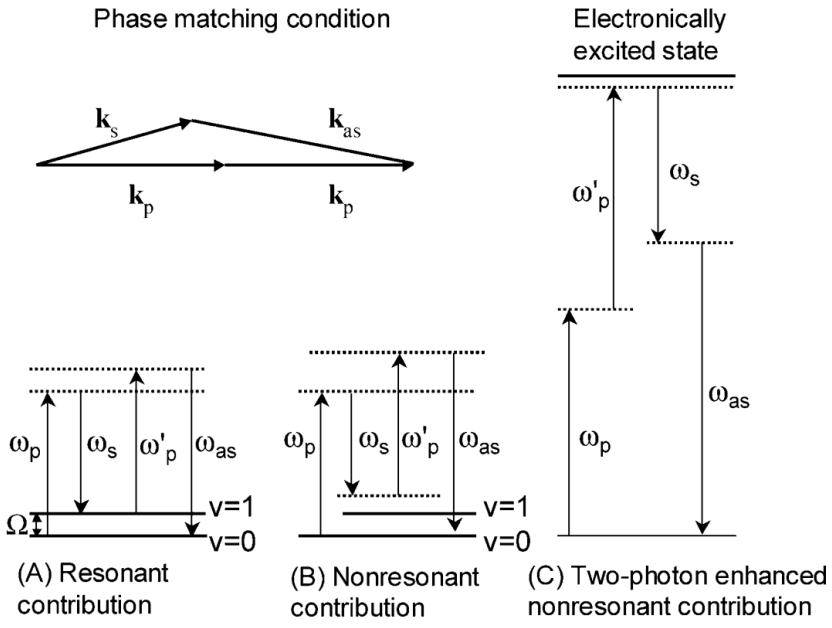

Figure 2.7: Energy diagram of CARS[3]

a small excitation volume. A CARS image is acquired by raster scanning the sample or the laser beams. The scattering process is resonantly enhanced when anti-Stokes frequency matches a molecular vibration of the sample.

The $\chi^{(3)}$ susceptibility for CARS is a combination of a resonant vibrational contribution and a non-resonant electronic term due to four-wave mixing. Given a detuning $\Delta = \omega_p - \omega_s - \omega_{vib}$ and a Raman line width Γ, the susceptibility is:

$$\chi^{(3)} = \chi^{(3)}_{NR} + \frac{\chi^{(3)}_R}{\Delta - i\Gamma}, \tag{2.9}$$

which results in a CARS line shape against a flat non-resonant background.

Since CARS intensity has a quadratic dependence on the pump beam intensity and a linear dependence on the Stokes beam intensity, the signal is gen-

erated from a small volume in the central focal region, providing CARS microscopy with a high 3D sectioning capability. The coherent summation of the CARS fields from a sizable sample leads to an intense and directional signal, which allows low excitation powers and fast scanning rates accordingly. Also since the signal frequency is blue-shifted, it can be easily detected in the presence of an one-photon fluorescence background [3].

2.3.2 Stimulated Raman Scattering Microscopy

Compared to CARS, SRS microscopy has the advantage of being background-free, where both pump and Stokes beams are incident on the sample. If the frequency difference $\Delta\omega = \omega_p - \omega_s$(known as the Raman shift) matches a molecular vibration of the sample, stimulated excitation of vibration transitions occurs and amplification of the Raman signal is achieved.

Compared to CARS microscopy, stimulated Raman scattering microscopy is independent from the non-resonant background. It also features a linear dependance on concentration.

However, since SRS microscopy detects the intensity change in pump signal or Stokes signal instead of detecting the new color, namely anti-Stokes light, it requires a super quiet source of synchronized pulses, which cannot yet be achieved by a fiber source without electronic noise cancellation.

CHAPTER 3

EXPERIMENTAL PROCESS

3.1 Building the Optical Parametric Amplifier

Before a close loop of fibers for the OPO structure is formed, an optical parametric amplifier (OPA) with a separate idler signal source at 1470nm needs to be built. A output signal at 800nm should be observed as proof of the desired four-wave mixing process inside PCF, meanwhile ruling out other experimental factors that possibly influence the functionality of OPO like coupling, PCF splice and divided pulse amplifier(DPA) in the future debugging process when building all-fiber OPO. A schematic is shown in Figure 3.1.

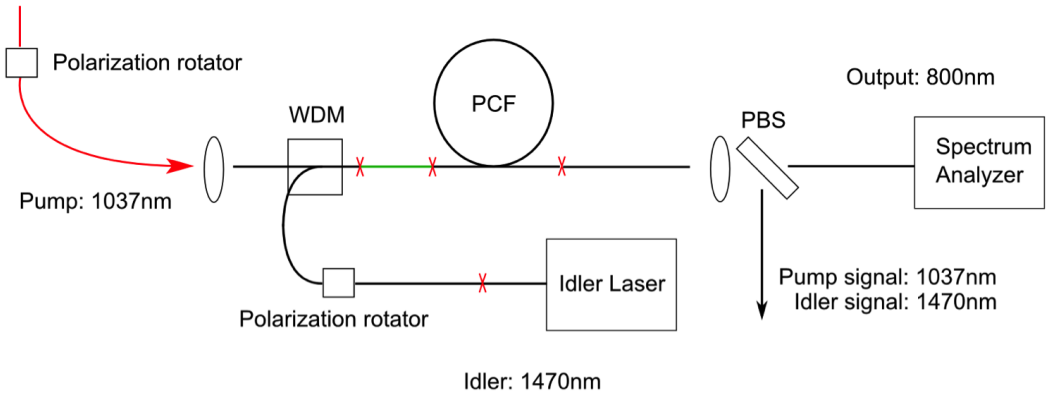

Figure 3.1: Schematic of all-fiber optical parametric amplifier

3.1.1 Preparation Work

First, the commercial laser and pump for DPA are set to working condition each time an experiment starts. The commercial laser is turned on, then its laser-

power button is pressed twice to rotate the laser medium so that possible bad spots in the gain medium could be avoided. After that, the LIMO Laser Diode Controller LDC1000 is turned on, then the Enter button is pressed to initiate temperature control. Within a few seconds, the temperature drops below 20.5°C, then the current is adjusted to 7A, laser-on button is pressed, and after a few seconds of stabilization the output signal of DPA reaches an average power of 110mW.

At this point, a 46.15MHz repetition rate pulse train at 1037nm with 6.6ps duration, 0.4nm bandwidth and 6.7nJ pulse energy is ready. This pulse train in the form of a free-space optical beam with 1mm diameter will be coupled into single-mode fiber(SMF) to pump the OPA/OPO through carefully chosen lens and stage. A lens with suitable focal length and maximum beam diameter is chosen so that the spot size at focal point is comparable to and slight smaller than fiber core size. The spot mode field diameter is given by:

$$\Phi_{spot} = \frac{4\lambda f}{\pi D}, \tag{3.1}$$

where f is the focal length of the lens, λ is the wavelength of the input light, and D is the diameter of collimated beam incident on the lens. Solving for the desired focal length of the collimating lens yields

$$f = \frac{\pi D(MFD)}{4\lambda} = \frac{\pi \times 1.0mm \times 6.1\mu m}{4 \times 1.03\mu m} = 4.6mm. \tag{3.2}$$

Based on this criterion, an LLO-4-4-λ lens with 4.6mm focal length and 4.8mm maximum beam diameter is picked. Since coupling a 1mm diameter Gaussian beam into a 10μm core size requires high precision, a NanoMax stage is used to fix cleaved fiber end and adjust its spacial position to the right spot in front of collimating lens. This 3-axis NanoMax stage has 0.5 mm/rev coarse adjustment and 50μm fine adjustment, which is suitable for this situation.

3.1.2 Beam Coupling

Before this beam goes into an optical fiber, it is reflected from two plane mirrors and then travels through the chosen collimating lens. To ensure that the beam hits the lens right through its optical axis, the NanoMax stage is placed after the second reflection mirror, and the lens is first replaced with a pinhole whose position is the same as the lens center. Then the two reflecting mirrors are adjusted such that the beam travels through the pinhole which can be examined by putting an IR-card behind the pinhole since this optical beam is at 1037nm wavelength and thus invisible to naked eyes but traceable by IR-card from florescence effect.

To track the beam's propagation direction, the IR-card is attached to a steel ruler, and hence if the ruler stands perpendicular against the optical table, the beam's spot on IR-card together with ruler's positions with respect to holes on the optical table tells the location of the beam. Ideally, the beam travels straight along x-direction with no y-direction and z-direction angle. To achieve this, the IR-card-attached ruler moves back and forth along a column of holes on the optical table, and tilting angles of the two reflecting mirrors are adjusted accordingly until the spot location stays still on the IR-card. Then the pinhole is replaced with the previously picked lens.

Both ends of the SMF shall be carefully cleaned and cleaved. The SMF lying in a slot on a metal stage is fixed on the NanoMax stage with screws and magnets, with its end a few millimeters from the collimating lens. The other end of the fiber is taped in front of a powermeter sensor to keep track of the amount of power passing through the fiber. The three axes of the stage are adjusted until an initial signal is detected. Then these three knobs are rotated in turns until the

signal is maximized. Assistance with infrared scope could help accelerate the process finding an initial signal.

Based on past experience, the coupling efficiency is around 65% - 70%. In this special case, the power after isolator is 102mW, and power detected after 1st WDM is 69mW, thus the total transmission of reflective mirros and lens coupling is:

$$\eta_{mirrors+coupling} = \frac{P_o}{P_i} = \frac{69mW}{102mW} = 68\%. \tag{3.3}$$

3.1.3 SMF-SMF and PCF-SMF Splice

Up to this point, the beam is able to collimate into fiber system, and what's left to be done is to complete the fiber OPA structure. The core consistent of this fiber OPA is the nonlinear medium, namely PCF. It is difficult to splice PCF directly with normal fiber due to large core size difference. We add HI1060 fiber with a slightly larger core between normal SMF and PCF so that the loss at splice points are minimized. Theoretically, power transmittance caused by core size difference is

$$T_0 = (\frac{2w_1w_2}{w_1^2 + w_2^2})^2. \tag{3.4}$$

The normal SMF-SMF splice is straightforward: clean and cleave the two fibers, then put both of then inside splicing machine within camera range, choose the default P01 program and let the machine finish alignment and splicing. The diode though, need to be sufficiently cleaned before each splice to lower splice failure rate. For HI1060-PCF splice, however, a special program coded P26 is written for this task. The program parameters initially come from Yuxing's program and are adjusted based on many following attempts. The detailed infor-

mation about this program is shown in the following Table 3.1:

Table 3.1: PCF-HI1060 Splice Program

Prefuse Time	0.3s
Prefuse Current	5mA
Gap	50μm
Overlap	1μm
Fusion Time 1	0.0s, -
Fusion Time 2	0.2s, 13mA
Fusion Time 3	0.0s, -
Set Center	205
AoA Current	6.5mA
Early Prefuse	No
Align Accuracy	0.05μm
Loss shift	0dB
Auto Center	No

The critical parameters of this program is fusion time and current. These numbers are carefully tuned through several attempts to both make PCF-HI1060 splice robust enough against minor vibrations and prevent air holes in PCF from collapsing. Note that this program is subject to adjustments based on the diode's status.

In our case, maximum possible efficiency predicted by power transmittance equation is:

$$T_{PCF-HI1060} = (\frac{2 \times 4.4\mu m \times 6.1\mu m}{(4.4\mu m)^2 + (6.1\mu m)^2})^2 = 90.0\%. \tag{3.5}$$

However, experimentally an output signal of 69mW from PCF is detected, mak-

ing transmission

$$\eta_{PCF-HI1060} = \frac{P_o}{P_i} = \frac{63mW}{69mW} = 91.3\%, \tag{3.6}$$

which slightly exceeds the predicted maximum value. This can be explained by a graduate decrease in mode field diameter at splice point from PCF to HI1060 fiber, since the previous formula applies to an abrupt MFD change situation.

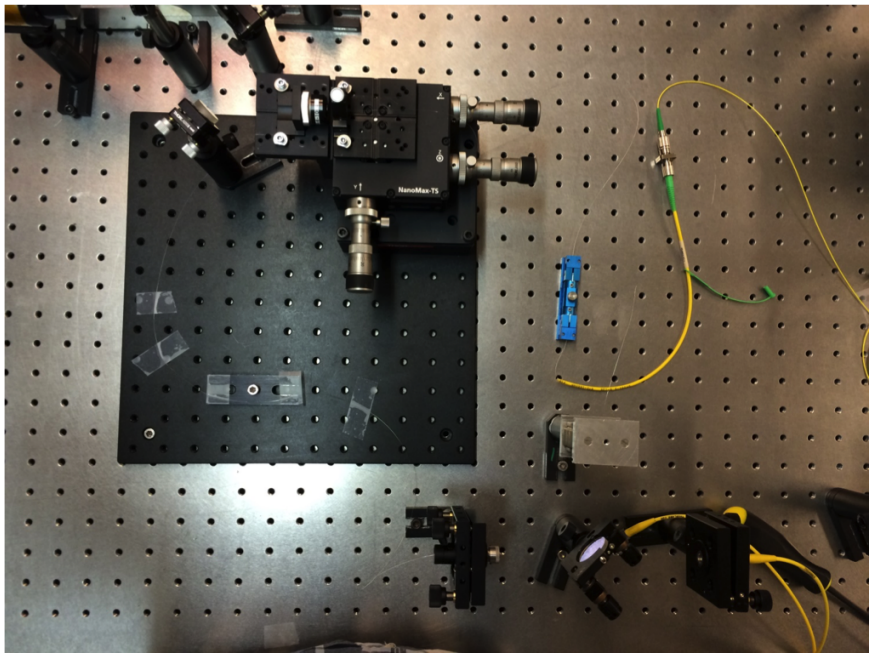

Figure 3.2: Setup of all-fiber optical parametric amplifier

3.1.4 External Idler Source

When the fiber components are connected as depicted in the schematic, adding idler signal source and polarization controller completes the OPA. A cw laser operating at 1470nm with tunable wavelength serves as the idler source for OPA and a polarization controller attached to its output matches the idler light polarization with input signal pulse polarization. The complete setup of this OPA is shown in Figure 3.2.

The output end of all-fiber OPA is attached to a fiber connector by cleaving the fiber by a few centimeters, pushing the bare fiber through the connector then cutting the extra fiber with a diamond knife. This connector, together with an adjustable lens, couple the light inside fiber back to a spacial beam. A dichroic mirror is placed at the output at 45° to the beam propagation direction, which reflects 1037nm light and transmits 800nm light so that these two colors could be separated.

At good phase matching condition, four wave mixing process is expected to occur within PCF, which can be proved by detecting light after the dichroic mirror, as shown in Figure 3.3.

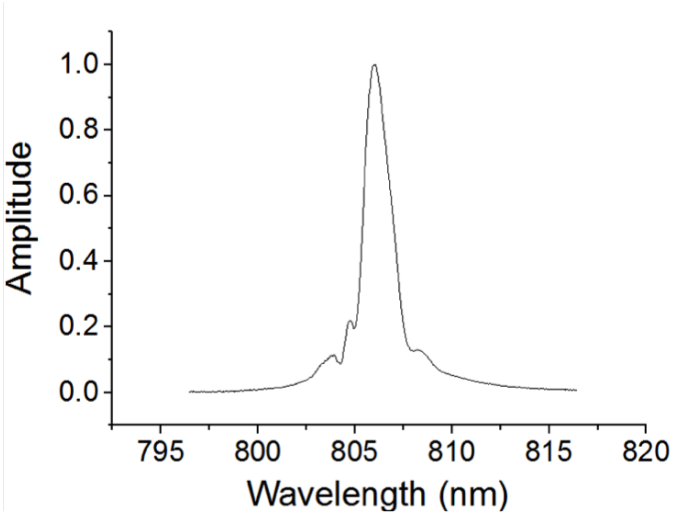

Figure 3.3: FWM signal spectrum from optical parametric amplifier

Once a FWM signal is confirmed for the OPA with outside idler input, the next step would be closing up the loop and make the FWM process self-consistent.

3.2 Building the Optical Parametric Oscillator

Up to this point, the OPA structure is complete. To form a closed loop for all-fiber OPO, more fiber components should be added, including a 2nd customized 1037/1470 WDM, delay line and spectral filter. The schematic of this OPO design is shown in Figure 3.4:

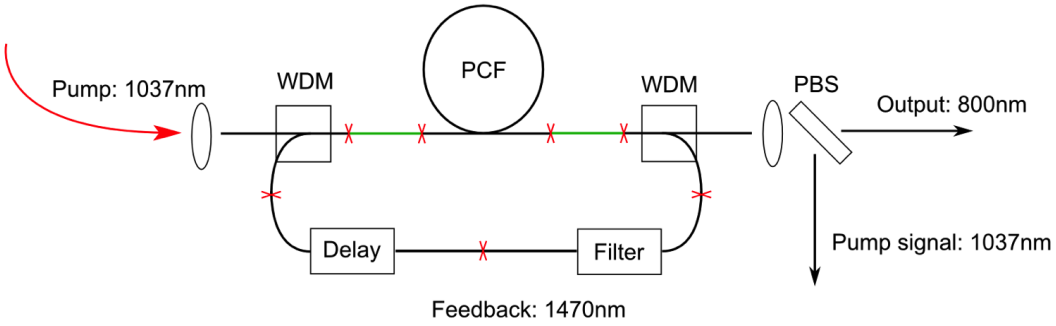

Figure 3.4: Schematic of all-fiber optical parametric oscillator

3.2.1 Close Loop Formation

One significant difference of this design compared to that of fiber OPA is that the external idler source is replaced with idler feedback. The 2nd WDM separates the idler signal generated by spontaneous FWM process inside PCF and sends it to a spectral filter. This tunable filter with bandwidth of about 2?nm selects the right frequency range and blocks other colors outside this regime so that only certain portion of the idler signal finishes the round trip and travels back into the PCF again to further seed the FWM process. Note that a polarization controller is added to the feedback loop so that after each roundtrip the idler polarization matches with pump light polarization. The complete all-fiber OPO

setup is shown in Figure 3.5.

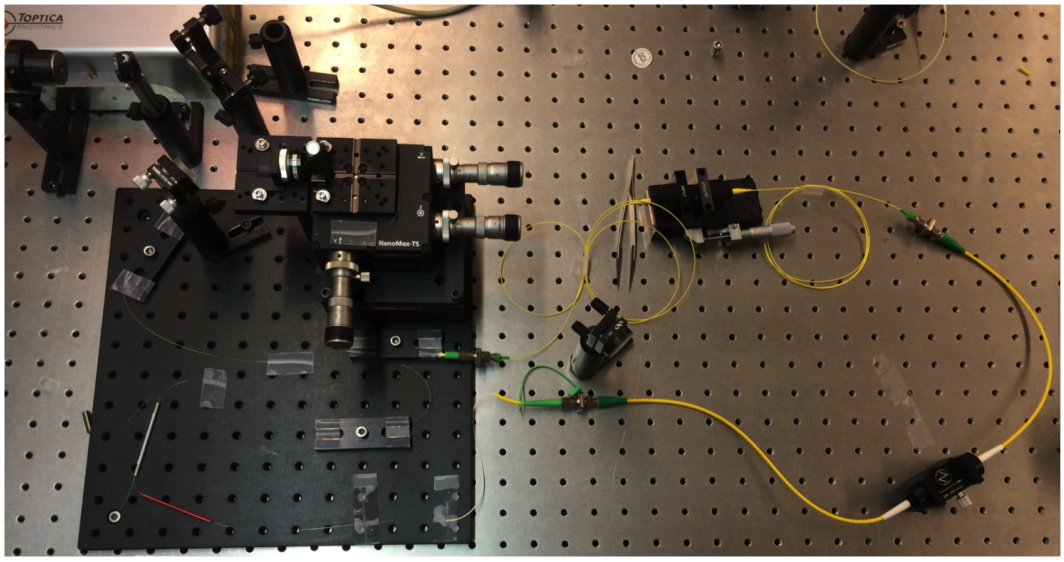

Figure 3.5: Setup of all-fiber optical parametric oscillator

3.2.2 Synchronization

The most important technical factor in building All-fiber OPO is that the optical path of fiber loop must match precisely with input pulse train repetition rate. In other words, one pulse should finishes the roundtrip inside fiber OPO system, seed back through the 1st WDM and overlap exactly with the next pulse. In order to achieve this, fiber loop length is carefully calculated as follows:

$$L_{loop} = \frac{c}{f_{rep} n_{core}} = \frac{3 \times 10^8 m/s}{46.15 \times 10^6 Hz \times 1.45} = 4.5m, \tag{3.7}$$

Since delay line and spectral filter components have fixed lengths of 2.30m and 0.68m, the only tunable length within this loop is HI1060. Starting from two spliced extra long HI1060 fibers, the delay line is scanned twice with different polarization status until a signal is picked behind dichroic mirror. If not,

redo the splice between these two HI1060 fibers to reduce the loop length by approximately 1.5cm, which is within delay line tunable range of 2.5cm. Note that optical path of the delay line tunable range is $D_{tune} \times n_{air} = 2.5 \times 1 = 2.5cm$, and fiber length loss caused by resplicing is $2 \times L_{cleave} \times n_{core} = 2 \times 0.8 \times 1.45 = 2.32cm$. The above steps are repeated a few times until a FWM signal is detected by powermeter.

3.3 Characterization and Optimization

Some factors to characterize the pulse train produced by all-fiber OPO including average power and repetition rate can either be directly measured by a powermeter or known by pumping pulse train. But for further information including bandwidth and duration, its spectral and temporal profile should be investigated.

3.3.1 Spectrum Measurement

After dichroic mirror, majority of the light is at around 800nm FWM signal. This signal is then re-coupled into a fiber connector through a non-tunable lens. The coarse alignment is done by directing the beam straight through the lens center without any x-direction or y-direction component relative to the beam's propagation direction, as roughly verified by a complete circle shape on IR-card which amplifies without much distortion when the IR-card is gradually moving away from the other side of the lens. For fine tuning, a fiber with small loss at 800nm wavelength is connected to the connector behind the lens, while the other end

of the fiber is fixed in front of a powermeter. The scrolls adjusting spacial orientation of the lens is carefully twisted until output power is maximized.

This fiber connector is then directly attached to a spectrum analyzer through which spectrum is scanned on a real-time basis. Spectrum span is adjusted to 10nm and central wavelength is set to 800nm, with power level set to reference power maximum.

The initial spectrum diagram is shown in Figure 3.6

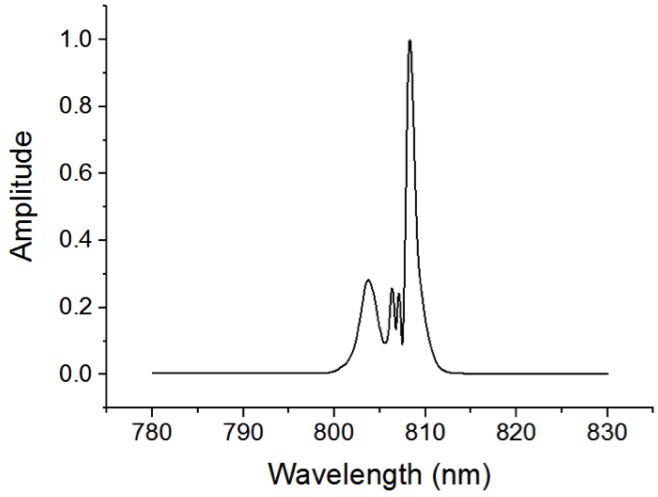

Figure 3.6: Initial OPO Signal Spectrum

3.3.2 Autocorrelation Measurement

To simultaneously record spectrum and autocorrelation, a flip mirror is placed such that the beam could switch from spectrum analyzer to autocorrelator with a single flip. After this flip mirror, this beam is then reflected from two more mirrors and passes through a half wave plate before entering the autocorrelator. The first mirror is adjusted to maximize the power at the entrance of autocorre-

lator, and then second mirror to correct optical path inside autocorrelator until the beam is split in two and hit both sides of the crystal where SHG could occur. Then several knobs are carefully twisted that correspond to wavelength, electrical level, etc., until the autocorrelation signal is maximized on the oscilloscope.

The raw data from autocorrelator is multiplied by a 46.5 interferometer factor and divided by a 1.5 deconvolution factor, then the full-width-half-maximum (FWHM) gives the actual duration of the measured pulse, assuming Gaussian fit.

The initial autocorrelation diagram is shown in Figure 3.7

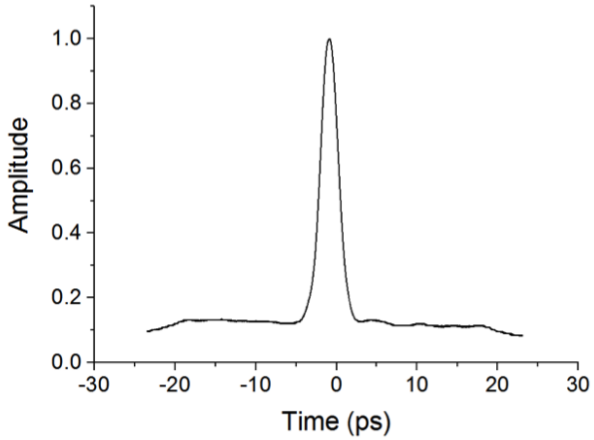

Figure 3.7: Initial OPO Signal Autocorrelation

3.3.3 Optimization

Optimization goes mainly in two directions: shorten PCF and shorten SMF before PCF. Too short PCF reduced efficiency of frequency conversion, while too long PCF encourages back conversion, so it is critical to reach a suitable length. Since we are using rare customized PCF provided by University of Bath, we

starts from an overlength PCF and reduces its length as slowly as possible, at an average rate of 0.8cm/cleave. On the other hand, the nonlinear length of this fiber system is around 10cm, and dispersion length is a lot longer than that; 30cm SMF before PCF, including inevitable WDM length, leads to 6π nonlinear phase accumulation, which could result in pulse shape distortion and thus reduce peak power, so we also reduce SMF before PCF gradually down to the lowest possible value of 17cm. Since fiber loop length is critical and should be carefully maintained, each fiber removal and addition including each cleave is recorded with precision down to sub-millimeter level.

Note that orientations of birefringent crystal in divided pulse amplifier (DPA) have significant impact on FWM signal spectrum shape and power. However, they are precisely aligned to maximize pulse amplification inside DPA, and thus their orientation should be recorded and kept still most of the time.

CHAPTER 4

DATA AND ANALYSIS

At PCF length of 26.9cm, a stable working state of the all-fiber with matching signal parameters is reached. The spectrum and autocorrelation dataset is published in [12], and shown in Figure 4.1 and Figure 4.2.

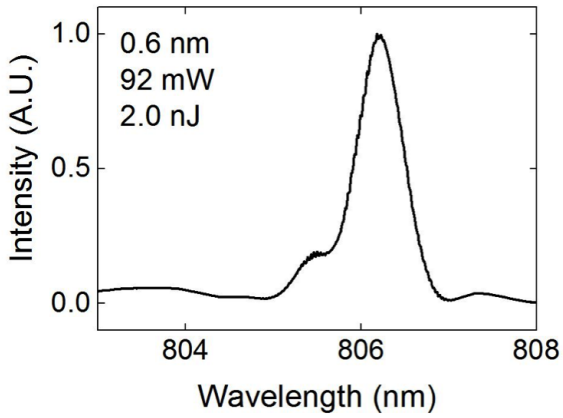

Figure 4.1: OPO Signal Spectrum, 26.9cm PCF

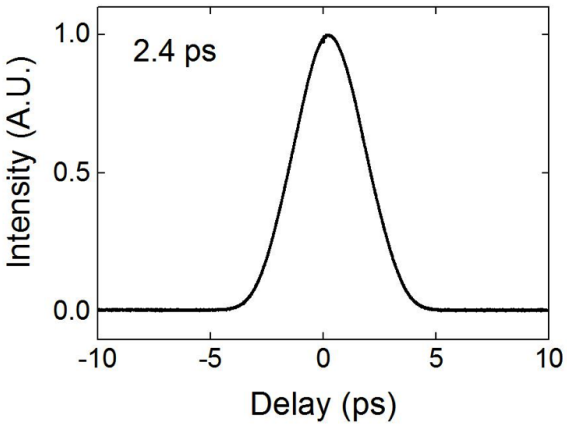

Figure 4.2: OPO Signal Autocorrelation, 26.9cm PCF

After that, the PCF is further cleaved and FWM signal power keeps increasing until stabilizing at around 19.6cm PCF length. This spectrum/autocorrelation dataset is announced at SPIE BiOS conference.

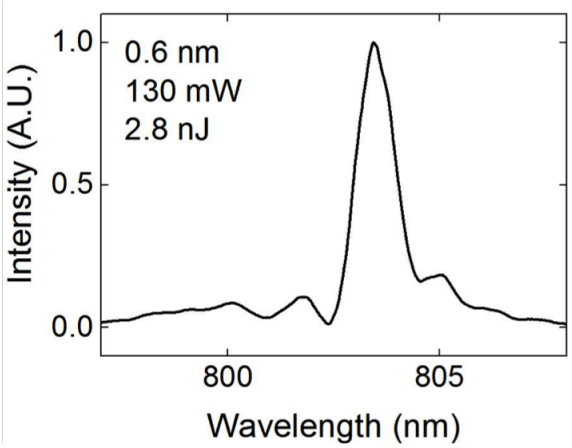

Figure 4.3: OPO Signal Spectrum, 19.6cm PCF

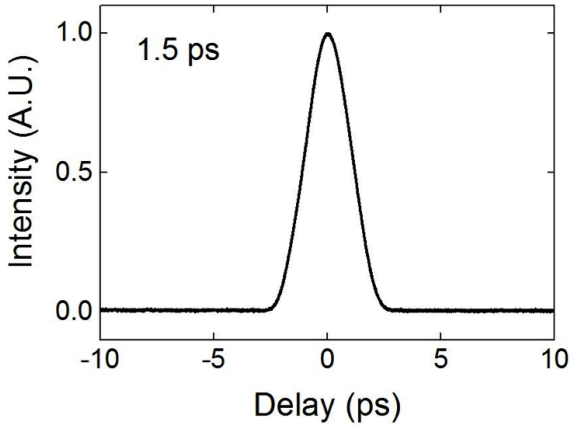

Figure 4.4: OPO Signal Autocorrelation, 19.6cm PCF

This all-fiber OPO generates 1.5ps duration, 0.6nm bandwidth pulses at 804nm with 2.8nJ pulse energy and 46.15MHz repetition rate, together with a synchronized pump pulse train at 1037nm. The signal pulse parameters have reached the same level of the previously developed PCF-based OPO [11]. These pulse trains meet all the requirements for CARS fiber source, subject to minor frequency tuning to match exactly with molecular vibration mode.

CHAPTER 5

CONCLUSION AND FUTURE WORK

In conclusion, we have built an all-fiber OPO that provides two synchronized pulse trains with right parameters for CARS microscopy. The schematic and experimental setup of the system is shown below:

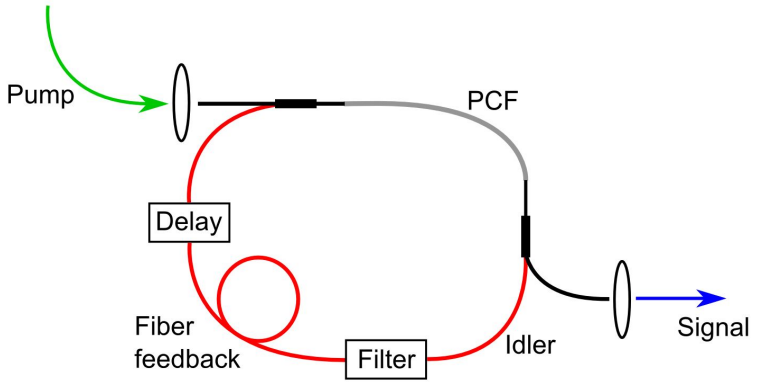

Figure 5.1: All-fiber OPO schematic

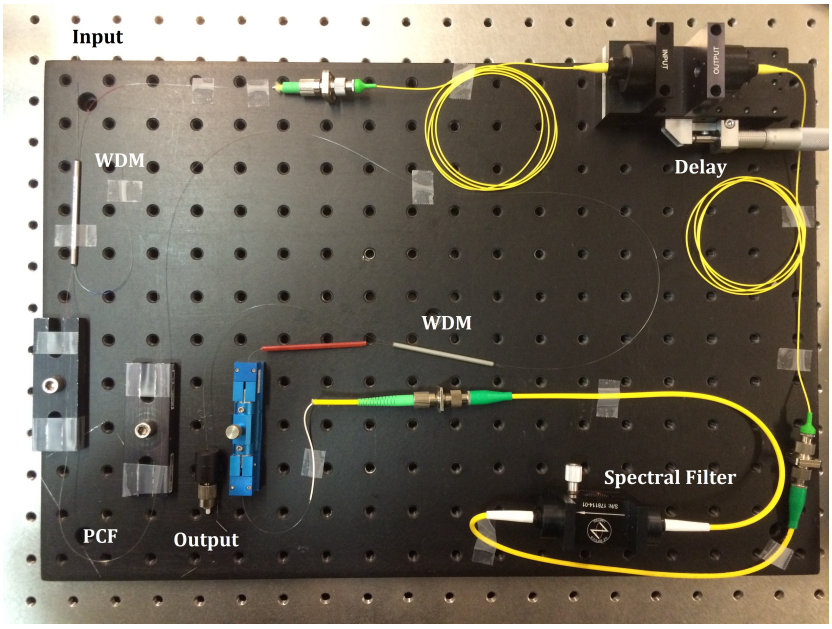

Figure 5.2: All-fiber OPO experimental setup

We have also measured the noise level of this all-fiber pumped by Picofyb commercial laser and DPA, as shown in Figure 5.3

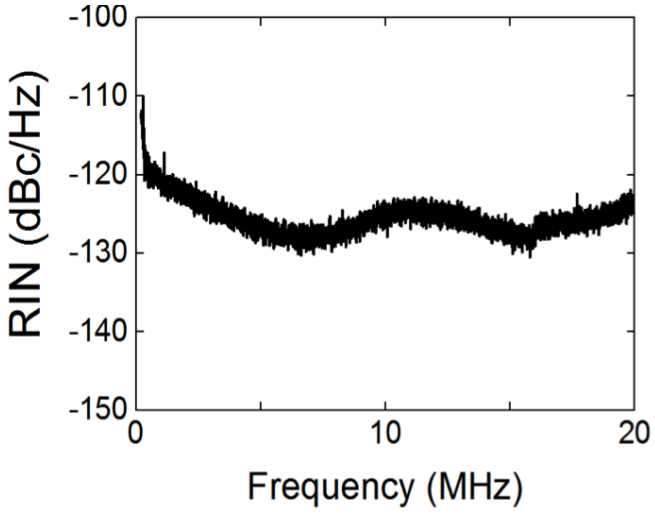

Figure 5.3: All-fiber OPO Relative Intensity Noise

Although this noise level is sufficient for CARS microscopy, but to extend this system to the background-free SRS imaging, the noise level is still too high above noise floor. So far, no fiber source has been reported to be naturally quiet enough for SRS imaging without electronic noise cancellation, and limited amount of attention has been paid to noise performance of fiber systems. We have observed the advantage of OPO over OPA in its noise level due to the self-consistent nature of OPO structure where random noise signals cancel each other after multiple round trips. Since the pumping laser generates a lot noise input, our group is currently developing a similariton amplifier fiber laser to pump the OPO which might potentially further reduce the noise level.

BIBLIOGRAPHY

[1] G. Agrawal. *Nonlinear Fiber Optics*. 2000.

[2] Robert W Boyd. *Nonlinear Optics*, volume 5. 2003.

[3] Ji-xin Cheng and X Sunney Xie. Coherent Anti-Stokes Raman Scattering Microscopy: Instrumentation, Theory, and Applications. *Journal of physics Chemical B*, 108(1):827–840, 2004.

[4] Yujun Deng, Qiang Lin, Fei Lu, Govind P Agrawal, and Wayne H Knox. Broadly tunable femtosecond parametric oscillator using a photonic crystal fiber. *Optics letters*, 30(10):1234–1236, 2005.

[5] Robert C. Eckardt, C. D. Nabors, William J. Kozlovsky, and Robert L. Byer. Optical parametric oscillator frequency tuning and control, 1991.

[6] Conor L Evans and X Sunney Xie. Coherent anti-stokes Raman scattering microscopy: chemical imaging for biology and medicine. *Annual review of analytical chemistry (Palo Alto, Calif.)*, 1:883–909, 2008.

[7] Christian W. Freudiger, Wenlong Yang, Gary R. Holtom, Nasser Peyghambarian, X. Sunney Xie, and Khanh Q. Kieu. Stimulated Raman scattering microscopy with a robust fibre laser source. *Nature Photonics*, 8(2):153–159, 2014.

[8] Feruz Ganikhanov, Silvia Carrasco, X Sunney Xie, Mordechai Katz, Wolfgang Seitz, and Daniel Kopf. Broadly tunable dual-wavelength light source for coherent anti-Stokes Raman scattering microscopy. *Optics letters*, 31(9):1292–1294, 2006.

[9] Thomas Gottschall, Tobias Meyer, Martin Baumgartl, Benjamin Dietzek, Jürgen Popp, Jens Limpert, and Andreas Tünnermann. Fiber-based optical parametric oscillator for high resolution coherent anti-Stokes Raman scattering (CARS) microscopy. *Optics Express*, 22(18):21921–21928, 2014.

[10] Khanh Kieu, Brian G Saar, Gary R Holtom, X Sunney Xie, and Frank W Wise. High-power picosecond fiber source for coherent Raman microscopy. *Optics letters*, 34(13):2051–2053, 2009.

[11] Erin S Lamb, Simon Lefrancois, Minbiao Ji, William J Wadsworth, X Sunney Xie, and Frank W Wise. Fiber optical parametric oscillator for coherent anti-Stokes Raman scattering microscopy. *Optics letters*, 38:4154–7, 2013.

[12] Erin S. Lamb, Hanzhang Pei, and Frank W. Wise. Towards low-noise fiber sources for coherent Raman microscopy. *SPIE BiOS*, 9329:932920, 2015.

[13] Simon Lefrancois. High Energy Pulse Propagation and Parametric Conversion in Normal-Dispersion Optical Fibers. *Diss. Cornell University*, (August), 2012.

[14] Simon Lefrancois, Dan Fu, Gary R. Holtom, Lingjie Kong, William J. Wadsworth, Patrick Schneider, Robert Herda, Armin Zach, X. Sunney Xie, and Frank W. Wise. Fiber four-wave mixing source for coherent anti-Stokes Raman scattering microscopy, 2012.

[15] P E Powers, R J Ellingson, W S Pelouch, and C L Tang. Recent Advances of the Ti-Sapphire-Pumped High-Repetition-Rate Femtosecond Optical Parametric Oscillator. *Journal of the Optical Society of America B-Optical Physics*, 10:2162–2167, 1993.

[16] S. D. Butterworth, W. A. Clarkson, N. Moore, G. J. Friel and D. C. Hanna. Synchronously pumping of an parametric oscillator using an amplified quasi-cw pump envelope. In *Advanced Solid State Lasers*, 1996.

[17] Brian G Saar, Christian W Freudiger, Jay Reichman, C Michael Stanley, Gary R Holtom, and X Sunney Xie. Video-rate molecular imaging in vivo with stimulated Raman scattering. *Science*, 330(6009):1368–70, 2010.

[18] T Südmeyer, J Aus der Au, R Paschotta, U Keller, P G Smith, G W Ross, and D C Hanna. Femtosecond fiber-feedback optical parametric oscillator. *Optics letters*, 26:304–306, 2001.